Journal of Neuroscience Methods 409 (2024) 110196

Contents lists available at ScienceDirect

Journal of Neuroscience Methods

journal homepage: www.elsevier.com/locate/jneumeth

Open cranium model for the study of cerebrovascular dynamics in intracranial hypertension

Rohan Jaishankar [a,b], Daniel Teichmann [a], Alison Hayward [c,d], James W. Holsapple [e], Thomas Heldt [a,b,*]

[a] Institute for Medical Engineering & Science, Massachusetts Institute of Technology, Cambridge, MA 02139, USA
[b] Department of Electrical Engineering & Computer Science, Massachusetts Institute of Technology, Cambridge, MA 02139, USA
[c] Division of Comparative Medicine, Massachusetts Institute of Technology, Cambridge, MA 02139, USA
[d] Department of Mechanical Engineering, Massachusetts Institute of Technology, Cambridge, MA 02139, USA
[e] Department of Neurosurgery, Boston University School of Medicine, Boston, MA 02118, USA

ARTICLE INFO

Keywords:
Intracranial pressure
Porcine model
Intracranial hypertension
Hemicraniectomy

ABSTRACT

Background: Significant research has been devoted to developing noninvasive approaches to neuromonitoring. Clinical validation of such approaches is often limited, with minimal data available in the clinically relevant elevated ICP range.
New Method: To allow ultrasound-guided placement of an intraventricular catheter and to perform simultaneous long-duration ICP and ultrasound recordings of cerebral blood flow, we developed a large unilateral craniectomy in a swine model. We also used a microprocessor-controlled actuator for intraventricular saline infusion to reliably and reversibly manipulate ICP according to pre-determined profiles.
Results: The model was reproducible, resulting in over 80 hours of high-fidelity, multi-parameter physiological waveform recordings in twelve animals, with ICP ranging from 2 to 78 mmHg. ICP elevations were reversible and reproducible according to two predetermined profiles: a stepwise elevation up to an ICP of 30–35 mmHg and return to normotension, and a clinically significant plateau wave. Finally, ICP was elevated to extreme levels of greater than 60 mmHg, simulating extreme clinical emergency.
Comparison with existing methods: Existing methods for ICP monitoring in large animals typically relied on burr-hole approaches for catheter placement. Accurate catheter placement can be difficult in pigs, given the thickness of their skull. Additionally, ultrasound is significantly attenuated by the skull. The open cranium model overcomes these limitations.
Conclusions: The hemicraniectomy model allowed for verified placement of the intraventricular catheter, and reversible and reliable ICP manipulation over a wide range. The large dural window additionally allowed for long-duration recording of cerebral blood flow velocity from the middle cerebral artery.

1. Introduction

Neurological disorders and injuries of the brain contribute significantly to the annual hospitalizations in the United States and globally (Gooch et al., 2017; Global Burden of Disease Neurology Collaborators, 2019; Taylor et al., 2017; Virani et al., 2020; Chin, 2014; Carney et al., 2017). Common conditions include traumatic brain injury, hemorrhagic stroke, hydrocephalus, cerebral malaria, and tuberculosis meningitis, all of which can result in elevation of intracranial pressure (ICP) and possible breakdown of cerebrovascular autoregulatory mechanisms, carrying the risk of fatal outcomes (Kochanek et al., 2019; Heldt et al., 2019). The expeditious monitoring and treatment of these disorders often involve the invasive measurement of ICP by placing a catheter in the cerebrospinal fluid (CSF) filled ventricular system or a pressure transducer placed in the brain parenchyma (Heldt et al., 2019). Several attempts have been made to develop novel noninvasive or minimally invasive neuromonitoring approaches and validate such methods against clinical gold-standard invasive measurements in neurocritical care patients (Heldt et al., 2019; Evensen and Eide, 2020; Hawryluk et al., 2022; Kashif et al., 2008, 2012). Given that the primary goal of

* Correspondence to: Institute for Medical Engineering & Science, Massachusetts Institute of Technology, Building E25-324, Cambridge, MA 02139, USA.
E-mail address: thomas@mit.edu (T. Heldt).

https://doi.org/10.1016/j.jneumeth.2024.110196
Received 10 November 2023; Received in revised form 16 March 2024; Accepted 10 June 2024
Available online 14 June 2024

neurocritical care is to stabilize the patient and normalize all key physiological variables, such clinical validation is often limited to the normal range of measured ICP. This limitation of human clinical data motivated the development of an animal model in which ICP can be manipulated in a controlled manner over a wide range and allows for extended-duration recordings of cerebrovascular and hemodynamic waveform data.

Here, a porcine model was chosen, as pigs have very similar cardiovascular and cerebrovascular anatomy to that of humans. Pigs also have vital signs and range of normal physiological parameters that are comparable to those of humans, and are sufficiently large to allow for standard hemodynamic and cerebrospinal instrumentation, similar to that used for humans in clinical neurocritical care. For these reasons, swine have also been used routinely in the past as experimental models for ischemic stroke (Allen et al., 2012; Arikan et al., 2017; Mangla et al., 2015; Brady et al., 2010; Elizondo et al., 2021; Govindan et al., 2019) and to investigate cerebrovascular autoregulation (Global Burden of Disease Neurology Collaborators, 2019; Janda et al., 2012; Kaiser and Fruhauf, 2007; Klein et al., 2019; Muench et al., 2007; Aquilina et al., 2007; Ciarrocchi et al., 2022).

Expanding on past work (Arikan et al., 2017; Mangla et al., 2015; Brady et al., 2010; Elizondo et al., 2021; Govindan et al., 2019; Janda et al., 2012; Klein et al., 2019; Muench et al., 2007; Ciarrocchi et al., 2022; Doron et al., 2020), we developed a stable, reproducible open-cranium model that allows for alteration of the cerebrospinal fluid state over a wide range, and multimodality monitoring of hemodynamic and cerebrovascular variables, in particular ICP, arterial blood pressure (ABP) and cerebral blood flow velocity (CBFV). The rich waveform data collected from these experiments can then be analyzed to validate, among other possibilities, the robustness of noninvasive ICP estimation methods over a wide range of measured ICP.

2. Materials and methods

All procedures and experiments were approved by MIT's Committee on Animal Care. We conducted extensive preparatory explorations on harvested tissue samples that guided our model development, such as sequential sectioning of frozen tissue samples and 3D MRI reconstructions of freshly harvested tissue samples (Supplementary Material Figures S1 and S2, respectively). The experimental protocol detailed here built on these detailed explorations.

2.1. Anesthesia and physiological stability maintenance protocol

All experiments were conducted on female Yorkshire pigs. Prior to the experiment, the animals were fasted overnight. On the day of the experiment, the animals were sedated with an intramuscular injection of 5 mg/kg telazol (tiletamine and zolazepam), 2 mg/kg xylazine and 0.06 mg/kg atropine. Once intravenous (IV) access was obtained percutaneously through an ear vein, endotracheal intubation was performed using a 7–0 endotracheal tube. Anesthesia was maintained using isoflurane (2–3 % in oxygen). The animals were placed on continuous IV fluid support (physiological saline) at a rate of 5 ml/kg/hr, adjusted for any blood loss, for the duration of the experiment. The animals were mechanically ventilated (DRE Veterinary AV-800 or Hallowell EMC Model 2000) in the controlled-volume setting with a tidal volume of 10–15 ml/kg and a respiratory rate set at 20 breaths per minute. Heated surgical tables and blankets were used to maintain a stable core body temperature. At the end of the experiment, the animals were euthanized with an IV injection of 390 mg/ml sodium pentobarbital.

2.2. Instrumentation

The animals were initially placed in dorsal recumbancy and instrumented for vital-sign measurement and hemodynamic monitoring. Surface electrocardiogram (ECG) leads were placed on the limbs in the standard three-lead configuration to monitor cardiac electrical activity. The tip of the ear or the inside of the lower jaw was used to monitor blood oxygenation levels (SpO_2) using a standard optical photoplethysmograph (PPG) sensor. Core body temperature was measured by inserting a temperature probe into the esophagus. Sidestream capnography was used to monitor $EtCO_2$ and respiratory rate. The femoral arteries were cannulated bilaterally under ultrasound guidance, and ABP was measured continuously from both sides using standard fluid-filled catheters. One of the femoral veins was also cannulated under ultrasound guidance for additional IV access. The carotid artery was cannulated via surgical cut-down to expose the carotid sheath. A 2 F Mikro-Tip catheter (Millar Instruments) was threaded approximately 5 cm into the carotid artery towards the heart to continuously record a high-fidelity carotid ABP signal closer to the brain's vasculature. Urine output was monitored by placement of a 12 F urinary catheter via a cystotomy. The ECG, SpO_2, temperature, capnogram, and one femoral ABP signal were displayed on a Cardell VetTrends V monitor for continuous surveillance of the animal's vital signs.

2.3. Craniectomy

Following induction of general anesthesia, intubation, and hemodynamic instrumentation, the animal was placed in the prone position on a warming pad. With the forelimbs flexed at the elbows with shoulders adducted, the head was positioned in a custom-built stereotaxic frame based on prior work (Poceta et al., 1981) with the neck slightly extended and the orbitomeatal line positioned horizontally. The head was secured in place by snout and ear bars placed in the mouth and external auditory canals, respectively. Adjustments were made to maintain the head in the horizontal position and centered in the head frame. The stereotaxic frame was crucial to stabilize the head of the animal for the craniectomy, to hold the ICP and TCD probes in place, and to serve as a reference for measurements of cranial landmarks.

The frontal, parietal, and temporal scalp was then shaved, and the midline marked in ink. An additional planning line was drawn perpendicular to the midline and extended approximately 8 cm just caudal to the lateral canthus on the operative side (Fig. 1a). A 10-blade was used to incise the scalp along the midline and laterally to expose the temporalis fascia. Raney clips were placed along the incision edges as needed to maintain hemostasis. Small perforating towel clamps were placed at the vertices of the scalp flaps that were reflected antero-inferiorly and postero-inferiorly and held in place with large rubber bands clamped to the nearby head appliance posts in the frame. Using monopolar cautery, the pericranium was dissected and removed from the superior surface of the exposed calvarium, and the attachment of the temporalis muscle along the temporal line was incised. The temporalis muscle was then undercut with monopolar cautery and removed in its entirety from the temporal fossa using rongeurs. In this fashion the temporal zygoma is exposed, and establishes the approximate superior-inferior level of the floor of the middle intracranial fossa (Fig. 1b).

A handheld, powered drill with an acorn cutting burr was used at high speed to thin (to < 1 mm) the frontal, parietal and temporal calvarium. Using Kerrison rongeurs, the inner cortex of the calvarium was then removed to expose the underlying and intact dura mater (Fig. 1c). A double action, thin point rongeur was then used to remove the lateral sphenoid and pterion, and expose the dural fold overlying the Sylvian fissure (Fig. 1d). Small cotton rolls were placed along the edges of the craniectomy in the epidural space to control epidural venous bleeding. The operative field was periodically irrigated with room temperature saline to remove any residual bone dust and blood, and gelfoam thrombin was used to control any bleeding from the bone.

2.4. ICP and CBFV measurements

Ultrasound imaging (CX-50, Philips Healthcare) was used to visualize the ventricular system, the inter-hemispheric fissure, and the

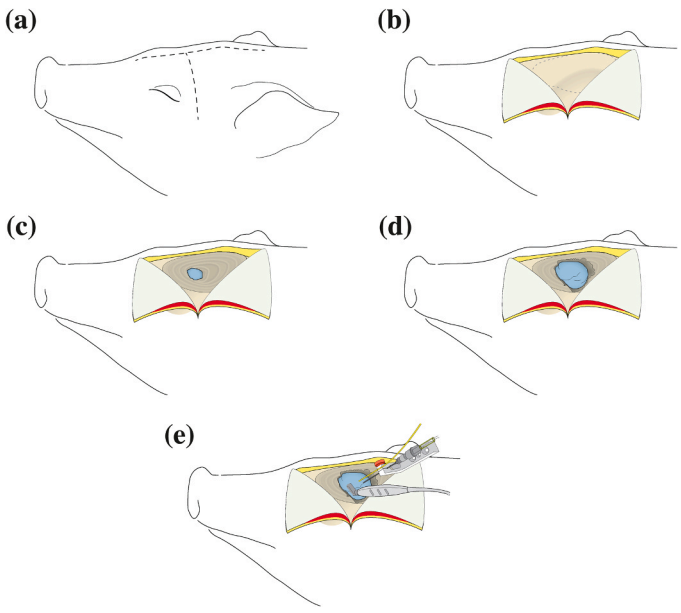

Fig. 1. Steps involved in the craniectomy procedure. Fig. 1a: Shaved head of prone animal with midline and planning line perpendicular to the midline marked. Incisions are made along these lines to expose the temporalis fascia. The animal's head is stabilized at all times by placing it in a custom stereotaxic frame. Fig. 1b: Temporal zygoma exposed by cutting down on the pericranium, and removing the temporalis muscle by monopolar cautery. The shaded region represents the original location of the excavated temporalis muscle, with the dotted boundary demarcating the exposed zygoma and the intracranial fossa. Fig. 1c: A small portion of the dura-covered brain is exposed (blue), after burring down on the frontal, parietal and temporal calvarium to thin it. The dura-covered brain is exposed by chipping the inner cortex of the calvarium away using a Kerrison punch. Fig. 1d: The lateral sphenoid and pterion are removed, and the exposure of the dural folds is extended until the Sylvian fissure. The craniectomy is complete at this stage. Fig. 1e: Once the dura-covered brain is exposed, two ICP monitoring probes, one intraventricular (black needle) and one intraparenchymal (yellow wire), are inserted with ultrasound guidance. A 4 MHz TCD probe is also placed on the dural folds to insonate the MCA. These probes are held in place by articulated fixtures, attached to the custom stereotaxic frame (Poceta et al., 1981).

lateral ventricle on the operative side (Fig. 2). An 18 G spinal needle with stylet in place was affixed to an articulated positioning arm, attached to the head frame, and positioned over the parietal dura. The needle angle was positioned to parallel the long axis of the ultrasound probe. With the lateral ventricle actively in view, the needle was

Fig. 2. Ultrasound image showing the target lateral ventricle in a porcine brain for placing an intraventricular ICP probe. Note this image was taken transdurally after a craniectomy to expose the dura-covered brain.

advanced to make contact with the dura. The dura of the planned puncture site was then coagulated using monopolar cautery, and the needle was slowly advanced under ultrasound guidance into the lateral ventricle. The stylet was then removed, and the needle attached to IV extension tubing and a 5 ml syringe filled with saline. A small amount of saline was injected, and the lateral ventricle visualized via ultrasound to confirm needle tip placement in the lateral ventricle and to demonstrate that the ventricular volume could be increased. Saline-filled extension tubing was then connected to a saline-primed three-way Luerlock stopcock, a pressure transducer, and IV fluid tubing maintained at body temperature and connected to an IV bag. Using a second spinal needle, a point on the dura 5 mm anterior to the ventricular catheter puncture site was coagulated and perforated. A calibrated 3.5 F Millar Mikro-Tip catheter was then placed through this dural puncture into the parietal brain parenchyma to a depth of 1–1.5 cm and secured in place, by attaching it to the articulated positioning arm holding the ventricular needle in place. Thus, pressure recordings from both the intraventricular catheter and parenchymal probe were obtained for ICP measurements.

A 4 MHz TCD ultrasound probe, connected to the DWL Doppler BoxX (Compumedics, USA), was then applied to the dural fold overlying the anterior-most Sylvian fissure, with generous amounts of ultrasound gel, to insonate the MCA. The probe was adjusted to obtain optimal CBFV signals from the MCA and held securely in place by a second articulated positioning arm from the frame (Fig. 1e). The operative field was gently irrigated with room-temperature saline and inspected for epidural bleeding which, if present, was controlled with cotton rolls and mild pressure. Additional ultrasound gel was gently added in small amounts to obtain a water seal at the parietal dural puncture sites, to ensure an accurate physiological ICP measurement was obtained at all times.

2.5. Data acquisition

Two ADInstruments eight-channel PowerLab 8/35 data acquisition systems were daisy-chained and used to record data streams from the multiple devices used throughout the experiment. The ECG, PPG, SpO_2, $EtCO_2$, respiratory rate, and one of the femoral ABP measurements were routed through the analog output of the veterinary monitor to the PowerLab for archiving. The other femoral ABP, the ventricular ICP (when transducing), the parenchymal ICP, and the carotid ABP waveforms were directly fed into the PowerLab. The MCA CBFV waveform was measured with the DWL Doppler BoxX, and the analog output was also streamed to the PowerLab for real-time CBFV archiving. All physiological waveforms were calibrated before the experiment and recorded on a common time axis, at a sampling rate of 1,000 samples/s and at an amplitude resolution of 16 bits. The heights of the femoral ABP transducers were adjusted to the same vertical level as the ICP transducer to eliminate any hydrostatic offsets in the pressure signals. Once all the instrumentation was complete, stable baseline data were collected for up to an hour.

2.6. Manipulation of intracranial pressure

Elevation of ICP was achieved by direct intraventricular infusion of saline at body temperature through the intraventricular port described previously. This amounts to an acute hydrocephalus model. A 1-liter saline bag was mounted on a height-adjustable IV stand and connected to the Luer lock of the intraventricular catheter through a standard IV tubing set. When the Luer lock was opened to the IV line, a hydrostatic column was established from the intraventricular space to the reservoir of the IV tubing line. As the reservoir was elevated vertically above the level of the ventricles, saline was infused into the ventricles and ICP rose until the inflow into the ventricles matched the outflow through the cerebrospinal fluid pathways.

To control the vertical height of the saline bag, the movable inner shaft of the IV stand was mechanically coupled to a linear actuator (JoyNano Nema 17) and controlled by a programmable microprocessor

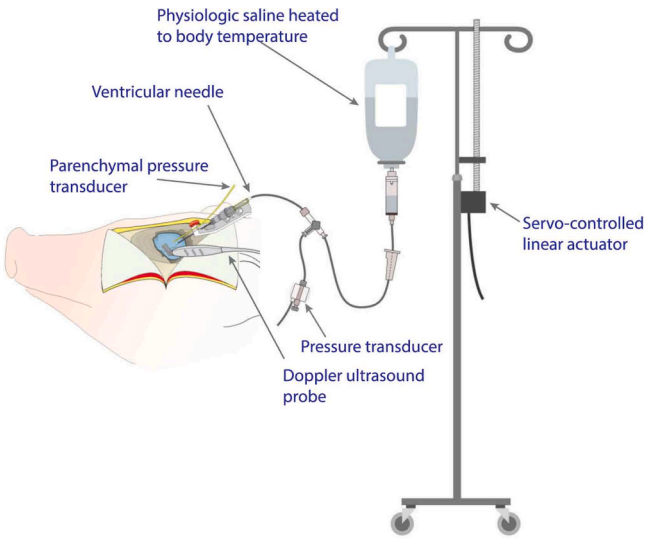

Fig. 3. Experimental approach to manipulating and measuring ICP. A servo-controlled linear actuator was programmed to elevate a saline bag in a pre-determined manner. The saline reservoir is connected to a needle whose tip is placed into the left lateral ventricle under ultrasonic guidance. Additionally, a solid-state pressure transducer is placed ~2 cm into the brain parenchyma.

(Arduino Uno R3). The actuator consisted of a stepper motor (1.8°/step; 8 mm/360° revolution) connected to the outer shaft with the lead screw connected to the inner shaft of the IV stand (Fig. 3). With the stepper motor engaged, the inner shaft of the IV stand, and hence the saline bag, were raised and lowered in a controllable manner. Assuming purely hydrostatic coupling, each 5 cm change in the vertical height of the saline bag should have resulted in a change in ICP of approximately 3.7 mmHg.

Two height-varying profiles were programmed. The first profile simulated a stepwise increase and subsequent decrease of ICP (Fig. 4a). The saline bag was elevated in steps of 5 cm at a time, up to a maximum of 30 cm above baseline ICP; the ICP was allowed to stabilize at each new level for 10 minutes. At the conclusion of the stepwise increase, the saline bag was lowered to baseline again in steps of 5 cm. This profile was chosen to probe the important transition zone in ICP from a normal ICP of about 5–10 mmHg to an elevated range of 30–35 mmHg, which would constitute a neurosurgical emergency when observed in humans. The second profile sought to mimic plateau waves commonly seen in neurotrauma patients (Hawryluk et al., 2022; Hayashi et al., 1991a, 1991b; Dias et al., 2014). For this, the stepper motor was programmed to elevate the saline bag at a constant speed of 5 cm/min to 30 cm above baseline ICP. The ICP was allowed to equilibrate at the maximum level for 10 minutes before the saline bag was returned, again at constant speed of 5 cm/min, to its baseline position (Fig. 4b). Finally, to simulate exceedingly high ICP values, in a subset of the animals the IV stand was disconnected from the stepper motor, and the inner shaft was manually elevated to achieve a maximum ICP of about 70 mmHg, depending on the hemodynamic stability of the animal (Fig. 4c).

2.7. Statistical analysis

The reproducibility of the ICP manipulations by controlled intraventricular saline infusion was tested across all animals. For each stepwise elevation profile, the baseline pre-elevation ICP was subtracted, and the changes in ICP produced by each vertical increase or decrease of 5 cm in the saline bag were noted. ICP changes of corresponding steps of 5 cm were then averaged across all such elevation profiles, after adjusting for any minor timing disparities. A mean stepwise elevation profile was computed, with a corresponding confidence band of one standard deviation across all elevation profiles. Similarly, a mean

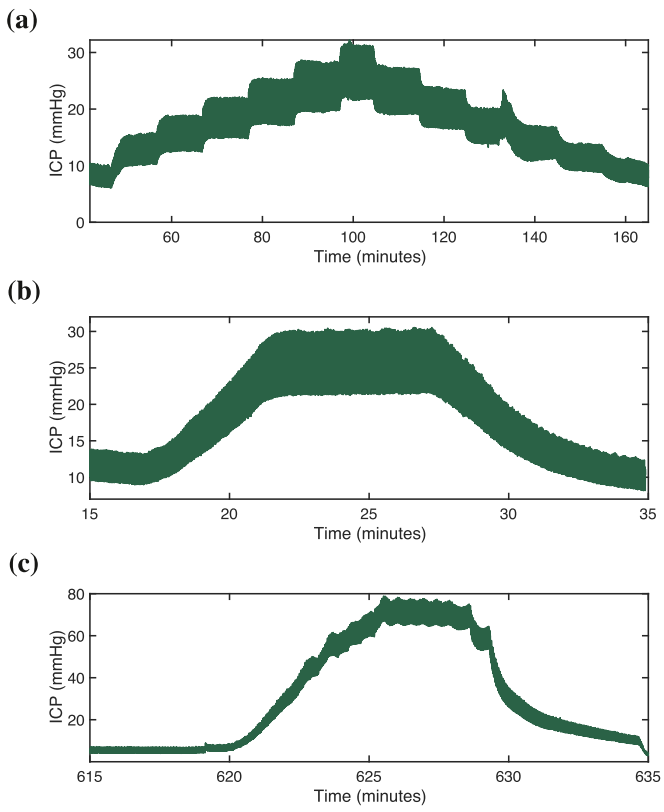

Fig. 4. Examples of ICP profiles implemented by pre-programmed intraventricular saline infusion (a, b) and manual elevation (c) of the IV stand on which the saline bag is mounted.(a) Example of pre-programmed stepwise elevation and reduction profile of ICP; (b) example of a pre-programmed plateau wave profile of ICP; these profiles were programmed into an Arduino Uno coupled to a stepper motor to control the vertical position of the IV bag coupled to the ventricular space. (c) Example of a manual elevation profile of ICP in which the vertical height of the saline bag was raised manually.

plateau-wave elevation profile was also computed, with the corresponding standard deviation.

3. Results

We studied twelve pigs, yielding around 80 hours of time-aligned physiological waveform data. All experiments were successfully completed without adverse complications. In two of the animals, the EVD was potentially misplaced, leading to minimal or unexpected variations in the mean ICP. Three of the animals exhibited dural bleeding at the point of EVD insertion, which was remedied by the topical application of gelfoam thrombin. The primary aim of the experiments was the elevation of ICP in a controlled manner, and this was successfully achieved in a reproducible manner with the three elevation protocols described earlier. The distribution of mean ICP measured in all the animals is shown in Fig. 4. The range of measured mean ICP was 2.1 mmHg to 78.2 mmHg, with an average of 17.7 mmHg and a standard deviation of 11. 3 mmHg. Around one third of all ICP measurements were over 22 mmHg, defined as the threshold for intracranial hypertension (Carney et al., 2017). A representative example of each of the elevation profiles is shown in Fig. 4. The reproducibility of the microprocessor-controlled stepper motor approach to generate the elevation profiles shown in Fig. 4a and Fig. 4b was tested, according to the statistical method described earlier. The results are shown in Fig. 6, where it can be seen that the approach was found to reproducibly elevate the ICP in a pre-programmed manner. It is important to note that the ICP measured during these elevations was lower than the theoretically predicted ICP at peak values (Fig. 6). This is because the

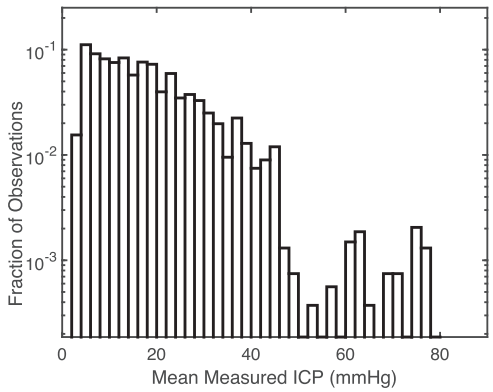

Fig. 5. Normalized distribution of mean measured ICP values across all animals. The range of the measured ICP in the porcine model dataset is 2.1 mmHg to 78.2 mmHg with a mean of 17.7 mmHg. Over 30 % of the measured mean ICP values are greater than 22 mmHg, commonly regarded as the threshold for elevated ICP (Carney et al., 2017).

intracranial chamber is an open fluid reservoir with outflow of the injected saline, but the resulting offset between observed and predicted ICP can be readily bridged using a closed-loop control system to adjust elevation of the IV stand (and thereby the ICP).

It is known that cerebral blood flow is determined by both the cerebral perfusion pressure, defined as the difference between the ABP and ICP, and the distributed biomechanical properties of the cerebral vasculature (primarily resistance and compliance). If the ICP exceeds the ABP, blood flow should cease due to vascular collapse. This phenomenon of cutoff of cerebral blood flow, an example of which is shown in Fig. 7, was verified in our experimental data. When the ICP was elevated to a level that exceeded the diastolic ABP, there was no diastolic blood flow through the MCA, as evidenced by the cutoff in the measured CBFV during the diastolic portion of the cardiac cycle. Conversely, once the ICP dropped below ABP, the CPP exceeded zero again, opening the vascular territory, resulting in resumption of cerebral blood flow. This result confirmed our understanding of the cerebrovascular physiology and validated our experimental approach.

4. Discussion

Due to the significant burden of neurological disorders and injuries worldwide, a large amount of research has been focused on improving and expanding the availability of techniques to monitor the neurological health of the patient. The assessment of candidate neuromonitoring approaches is often limited by the limited range of measured ICP and

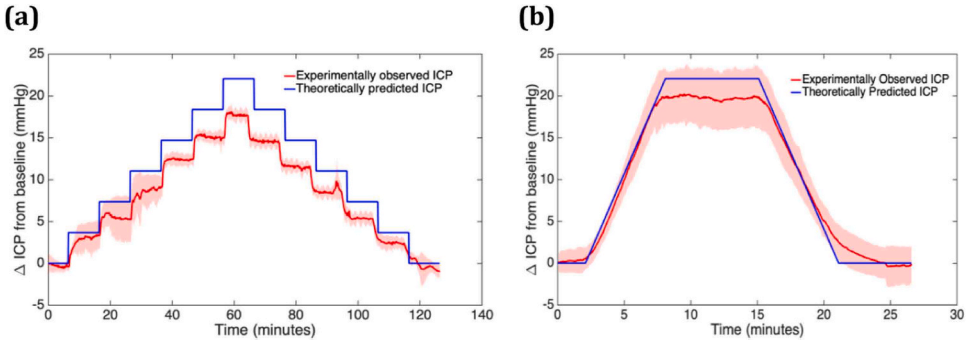

Fig. 6. Expected (blue) and measured (red) ICP profiles for the pre-programmed stepwise ICP profile (a) and plateau wave (b) manipulations. The plots describe the mean characteristics for 10 stepwise elevation and 13 plateau wave profiles in 9 pigs. The solid red line represents the mean changes in measured ICP across all such elevation profiles, with the shaded confidence regions representing one standard deviation around the mean change in measured ICP. The blue line represents the expected ICP profile based on the vertical height of the saline bag and assuming a purely hydrostatic coupling between the saline reservoir and the ventricular space.

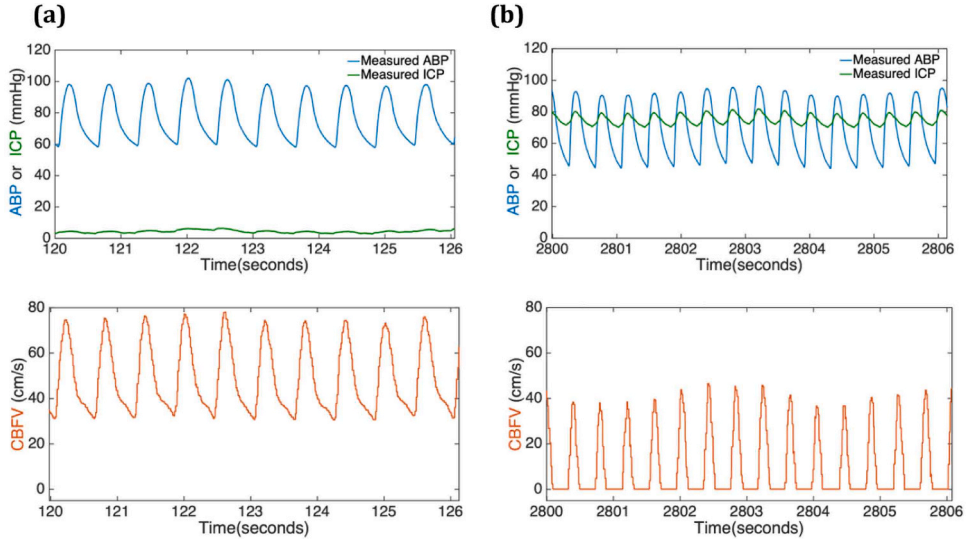

Fig. 7. Representative examples of arterial blood pressure (ABP), intracranial pressure (ICP), and cerebral blood flow velocity (CBFV) waveforms. (a) Example of intracranial normotension in which ABP far exceeds ICP; (b) Example of severe intracranial hypertension in which ICP exceeds ABP during the diastolic phase of the cardiac cycle with corresponding cerebral diastolic flow cut-off.

lack of significant trends in the ICP waveform data (Fanelli et al., 2019; Jaishankar et al., 2019, 2020; Imaduddin et al., 2020). As a result, there has been a need to establish a robust, reliable, and reproducible large-animal model to record physiological waveform data across a wide range of ICP values and with sufficient variation in the cerebrospinal state to allow for testing of novel candidate neuromonitoring hypotheses and devices.

Our work here, directly motivated by this inherent problem in using patient data, resulted in the development and implementation a porcine model to record physiological waveform data over a wide range of hemodynamic cerebrospinal states. Rather than opting for burr holes for placement of intracranial probes to either measure or manipulate ICP (through balloon inflation or saline infusion) (Sousa et al., 2016; Jeng et al., 2021; Soares et al., 2021; Twedt et al., 2017; Freimann et al., 2013; Metzger et al., 2018; Tiba et al., 2022; Ruesch et al., 2021, 2020), we opted for a sizeable unilateral craniectomy approach to expose the intact dura. Our choice was necessitated by the comparatively thick skull of adult Yorkshire swine and motivated by the need to visualize and expose the sphenoid wing of the Sylvain fissure, find the MCA, and obtain Doppler-based flow velocity recordings from the MCA for many hours. Additionally, the hemicraniectomy approach allowed us to visualize the ventricles, place the ventricular catheter under ultrasonic guidance, verify its placement by visualizing the ventricular expansion during instillation of fluid into the ventricles, and ultimately manipulate ICP through saline infusion. Since clinically, large craniectomies are typically performed deliberately to reduce ICP, it was not clear whether it was possible to manipulate ICP reproducibly and robustly over a wide range in a model that utilizes large craniectomies. Prior work using intact-dura craniectomies in swine either focused on providing a comparatively small access window for ultrasonography (Shin et al., 2022) or required dural access to apply controlled cortical impact for traumatic injury induction. In both studies, the ICP was only varied over a narrow range, and hence could not serve as a reference for our work.

We were able to record data from twelve pigs and obtained over 80 hours of time-aligned multi-parameter physiological waveform data, which is larger than what is reported in typical clinical cohorts (Evensen and Eide, 2020; Ciarrocchi et al., 2022; Doron et al., 2020; Fanelli et al., 2019; Jaishankar et al., 2019, 2020; Imaduddin et al., 2020). Additionally, we were able to reproducibly simulate two different ICP elevation profiles: a stepwise elevation and subsequent decrease of ICP (in steps of ~4 mmHg) in the important transitional range between intracranial normotension and overt intracranial hypertension; and a plateau wave (with ICP reaching 78 mmHg). As a result, a significant fraction of our recorded ICP data lies in the range of elevated ICP or intracranial hypertension (defined as ICP>22 mmHg (Carney et al., 2017); Kochanek et al., 2019). The resulting rich dataset also allows for a more rigorous quantification of candidate neuromonitoring approaches. Additionally, the elevation profiles used allow for evaluation of neuromonitoring techniques during dynamic changes in ICP, not just at different steady-state values.

Past work has also focused on the use of several cerebral autoregulation metrics as indicators of neurological health (Heldt et al., 2019; Hawryluk et al., 2022; Kaiser and Fruhauf, 2007; Klein et al., 2019; Armstead, 2016). These metrics focus on capturing the interplay between cerebral ABP and ICP, as mediated by several autoregulatory mechanisms, to maintain cerebral perfusion at constant and acceptable levels (Steiner et al., 2002). These mechanisms break down in cases of intracranial hypertension, leading to rapid decompensation and potentially herniation of the brain stem, and death. Hence, gaining insights into these metrics and predicting these acute episodes of elevated ICP that may require immediate surgical intervention is crucial. Our diverse dataset, with controlled and significant variations in ICP, and where the cerebral autoregulatory reserves of the animal are stressed, enables further investigations of these control mechanisms. Moreover, the manual ICP elevation profile depicted in Fig. 4c resulted in extreme levels of intracranial hypertension (ICP>50 mmHg), which would necessitate surgical intervention for sustenance of life in humans.

While our large craniectomy model allows for probing of intracranial dynamics over a wide range of cerebrovascular states, there is still scope for modifying the model to gain valuable information. Specifically, the variation of the hemodynamic state of the animal can be further explored through administration of vasoactive drugs or by altering the ventilation parameters. Similarly, the effect of various anesthetic drugs on the cerebral vasculature and the autoregulatory mechanisms can also be studied further (Dagal and Lam, 2009). Finally, while some the autoregulatory metrics reported in literature are indicators of the neurological health of the patient, the time-scale of the processes underlying these control mechanisms and their interplay are still debated in literature. The trends in ICP afforded by our animal model, measured with high temporal resolution, can be leveraged to potentially gain insights into these unanswered questions.

CRediT authorship contribution statement

Alison Hayward: Conceptualization, Data curation, Investigation, Methodology, Project administration, Validation, Writing – original draft, Writing – review & editing. **James W. Holsapple:** Writing – review & editing, Writing – original draft, Conceptualization, Data curation, Investigation, Methodology, Validation. **Thomas Heldt:** Validation, Supervision, Resources, Project administration, Methodology, Investigation, Funding acquisition, Formal analysis, Data curation, Conceptualization, Writing – original draft, Writing – review & editing. **Rohan Jaishankar:** Writing – review & editing, Writing – original draft, Validation, Methodology, Investigation, Formal analysis, Data curation. **Daniel Teichmann:** Writing – review & editing, Writing – original draft, Validation, Methodology, Investigation.

Declaration of Competing Interest

None.

Data availability

Data will be made available on request.

Acknowledgments

The authors wish to thank Ms. Keiko Ishida, Mr. Stuart Dillon Powell, and Ms. Taylor Baum for help during the experiments. We wish to thank Dr. Balasundar Raju, Dr. Jonathan Sutton and Dr. Jonathan Fincke of Philips Research North America for their help visualizing the animals' ventricular system ultrasonically. Additionally, we wish to thank Prof. Eun Bo Shim of Kangwon National University, Republic of Korea, for his help rendering and segmenting MRI images during preliminary explorations of the intracranial anatomical relationships. Finally, we wish to thank Mr. Kenneth Pierce for developing the illustrations of the surgical approach. This work was supported by Philips Research North America and a postdoctoral fellowship grant by Deutsche Forschungsgemeinschaft (DFG, German Research Foundation) under Grant TE 1174/2–1 to Dr. Teichmann.

Appendix A. Supporting information

Supplementary data associated with this article can be found in the online version at doi:10.1016/j.jneumeth.2024.110196.

References

Allen, B.S., Ko, Y., Buckberg, G.D., Sakhai, S., Tan, Z., 2012. Studies of isolated global brain ischaemia: i. A new large animal model of global brain ischaemia and its baseline perfusion studies. Eur. J. Cardiothorac. Surg. 41 (5), 1138–1146.

Aquilina, K., Hobbs, C., Cherian, S., Tucker, A., Porter, H., Whitelaw, A., et al., 2007. A neonatal piglet model of intraventricular hemorrhage and posthemorrhagic ventricular dilation. J. Neurosurg. 107 (2 Suppl), 126–136.
Arikan, F., Martinez-Valverde, T., Sanchez-Guerrero, A., Campos, M., Esteves, M., Gandara, D., et al., 2017. Malignant infarction of the middle cerebral artery in a porcine model. A pilot study. PLoS One 12 (2), e0172637.
Armstead, W.M., 2016. Cerebral blood flow autoregulation and dysautoregulation. Anesth. Clin. 34 (3), 465–477.
Brady, K.M., Mytar, J.O., Kibler, K.K., Hogue Jr., C.W., Lee, J.K., Czosnyka, M., et al., 2010. Noninvasive autoregulation monitoring with and without intracranial pressure in the naive piglet brain. Anesth. Analg. 111 (1), 191–195.
Carney, N., Totten, A.M., O'Reilly, C., Ullman, J.S., Hawryluk, G.W., Bell, M.J., et al., 2017. Guidelines for the management of severe traumatic brain injury, fourth edition. Neurosurgery 80 (1), 6–15.
Chin, J.H., 2014. Tuberculous meningitis: diagnostic and therapeutic challenges. Neurol. Clin. Pr. 4 (3), 199–205.
Ciarrocchi, N.M., Pose, F., Saez, P., Garcia, M.D.C., Padilla, F., Pedro, P., et al., 2022. Reversible focal intracranial hypertension swine model with continuous multimodal neuromonitoring. J. Neurosci. Methods 373, 109561.
Dagal, A., Lam, A.M., 2009. Cerebral autoregulation and anesthesia. Curr. Opin. Anaesthesiol. 22 (5), 547–552.
Dias, C., Maia, I., Cerejo, A., Varsos, G., Smielewski, P., Paiva, J.A., et al., 2014. Pressures, flow, and brain oxygenation during plateau waves of intracranial pressure. Neurocrit Care 21 (1), 124–132.
Doron, O., Barnea, O., Stocchetti, N., Or, T., Nossek, E., Rosenthal, G., 2020. Cardiac-gated intracranial elastance in a swine model of raised intracranial pressure: a novel method to assess intracranial pressure-volume dynamics. J. Neurosurg. 134 (5), 1650–1657.
Elizondo, L.I., Vu, E.L., Kibler, K.K., Rios, D.R., Easley, R.B., Andropoulos, D., et al., 2021. Critical closing pressure by diffuse correlation spectroscopy in a neonatal piglet model. Acta Neurochir. Suppl. 131, 295–299.
Evensen, K.B., Eide, P.K., 2020. Measuring intracranial pressure by invasive, less invasive or non-invasive means: limitations and avenues for improvement. Fluids Barriers CNS 17 (1), 34.
Fanelli, A., Vonberg, F.W., LaRovere, K.L., Walsh, B.K., Smith, E.R., Robinson, S., et al., 2019. Fully automated, real-time, calibration-free, continuous noninvasive estimation of intracranial pressure in children. J. Neurosurg. Pedia 1–11.
Freimann, F.B., Chopra, S.S., Unger, J.K., Vajkoczy, P., Wolf, S., 2013. Evaluation of a new large animal model for controlled intracranial pressure changes induced by capnoperitoneum. Acta Neurochir. 155 (7), 1345–1349.
Global Burden of Disease Neurology Collaborators, 2019. Global, regional, and national burden of neurological disorders, 1990-2016: a systematic analysis for the global burden of disease study 2016. Lancet Neurol. 18 (5), 459–480.
Gooch, C.L., Pracht, E., Borenstein, A.R., 2017. The burden of neurological disease in the United States: a summary report and call to action. Ann. Neurol. 81 (4), 479–484.
Govindan, R.B., Brady, K.M., Massaro, A.N., Perin, J., Jennings, J.M., DuPlessis, A.J., et al., 2019. Comparison of frequency- and time-domain autoregulation and vasoreactivity indices in a piglet model of hypoxia-ischemia and hypothermia. Dev. Neurosci. 1–13.
Hawryluk, G.W.J., Citerio, G., Hutchinson, P., Kolias, A., Meyfroidt, G., Robba, C., et al., 2022. Intracranial pressure: current perspectives on physiology and monitoring. Intensive Care Med. 48 (10), 1471–1481.
Hayashi, M., Handa, Y., Kobayashi, H., Kawano, H., Ishii, H., Hirose, S., 1991a. Plateau-wave phenomenon (I). Correlation between the appearance of plateau waves and CSF circulation in patients with intracranial hypertension. Brain 114 (Pt 6), 2681–2691.
Hayashi, M., Kobayashi, H., Handa, Y., Kawano, H., Hirose, S., Ishii, H., 1991b. Plateau-wave phenomenon (II). Occurrence of brain herniation in patients with and without plateau waves. Brain 114 (Pt 6), 2693–2699.
Heldt, T., Zoerle, T., Teichmann, D., Stocchetti, N., 2019. Intracranial pressure and intracranial elastance monitoring in neurocritical care. Annu Rev. Biomed. Eng. 21, 523–549.
Imaduddin, S.M., Fanelli, A., Vonberg, F.W., Tasker, R.C., Heldt, T., 2020. Pseudo-bayesian model-based noninvasive intracranial pressure estimation and tracking. IEEE Trans. Biomed. Eng. 67 (6), 1604–1615.
Jaishankar, R., Fanelli, A., Filippidis, A., Vu, T., Holsapple, J., Heldt, T., 2019. A frequency-domain approach to noninvasive intracranial pressure estimation. Annu Int Conf. IEEE Eng. Med. Biol. Soc. 2019, 5055–5058.
Jaishankar, R., Fanelli, A., Filippidis, A., Vu, T., Holsapple, J., Heldt, T., 2020. A spectral approach to model-based noninvasive intracranial pressure estimation. IEEE J. Biomed. Health Inf. 24 (8), 2398–2406.
Janda, M., Bajorat, J., Simanski, O., Noldge-Schomburg, G., Hofmockel, R., Schutze, M., 2012. A surgical technique for a terminal intracranial hypertension model in pigs. Lab Anim. 46 (3), 258–260.
Jeng, B.C.P., de Andrade, A.F., Brasil, S., Bor-Seng-Shu, E., Belon, A.R., Robertis, M., et al., 2021. Estimation of intracranial pressure by ultrasound of the optic nerve sheath in an animal model of intracranial hypertension. J. Clin. Neurosci. 86, 174–179.
Kaiser, G.M., Fruhauf, N.R., 2007. Method of intracranial pressure monitoring and cerebrospinal fluid sampling in swine. Lab Anim. 41 (1), 80–85.
Kashif, F.M., Heldt, T., Verghese, G.C., 2008. Model-based estimation of intracranial pressure and cerebrovascular autoregulation. Comput. Cardiol. 35, 369–372.
Kashif, F.M., Verghese, G.C., Novak, V., Czosnyka, M., Heldt, T., 2012. Model-based noninvasive estimation of intracranial pressure from cerebral blood flow velocity and arterial pressure. Sci. Transl. Med 4 (129), 129ra144.
Klein, S.P., De Sloovere, V., Meyfroidt, G., Depreitere, B., 2019. Autoregulation assessment by direct visualisation of pial arterial blood flow in the piglet brain. Sci. Rep. 9 (1), 13333.
Kochanek, P.M., Tasker, R.C., Carney, N., Totten, A.M., Adelson, P.D., Selden, N.R., et al., 2019. Guidelines for the management of pediatric severe traumatic brain injury, third edition: update of the brain trauma foundation guidelines, executive summary. Pedia Crit. Care Med. 20 (3), 280–289.
Mangla, S., Choi, J.H., Barone, F.C., Novotney, C., Libien, J., Lin, E., et al., 2015. Endovascular external carotid artery occlusion for brain selective targeting: a cerebrovascular swine model. BMC Res. Notes 8, 808.
Metzger, A., Mulligan, J., Grudic, G., 2018. Development of a non-invasive cerebrovascular status algorithm to estimate cerebral perfusion pressure and intracranial pressure in a porcine model of focal brain injury. Mil. Med. 183 (suppl_1), 119–123.
Muench, E., Horn, P., Bauhuf, C., Roth, H., Philipps, M., Hermann, P., et al., 2007. Effects of hypervolemia and hypertension on regional cerebral blood flow, intracranial pressure, and brain tissue oxygenation after subarachnoid hemorrhage. Crit. Care Med. 35 (8), 1844–1851 quiz 52.
Poceta, J.S., Hamlin, M.N., Haack, D.W., Bohr, D.F., 1981. Stereotaxic placement of cannulae in cerebral ventricles of the pig. Anat. Rec. 200 (3), 349–356.
Ruesch, A., Acharya, D., Schmitt, S., Yang, J., Smith, M.A., Kainerstorfer, J.M., 2021. Comparison of static and dynamic cerebral autoregulation under anesthesia influence in a controlled animal model. PLoS One 16 (1), e0245291.
Ruesch, A., Yang, J., Schmitt, S., Acharya, D., Smith, M.A., Kainerstorfer, J.M., 2020. Estimating intracranial pressure using pulsatile cerebral blood flow measured with diffuse correlation spectroscopy. Biomed. Opt. Express 11 (3), 1462–1476.
Shin, S.S., Sridharan, A., Khaw, K., Hallowell, T., Morgan, R.W., Kilbaugh, T.J., et al., 2022. Intracranial pressure and cerebral hemodynamic monitoring after cardiac arrest in pediatric pigs using contrast ultrasound-derived parameters. J. Ultrasound Med. 41 (6), 1425–1432.
Soares, M.S., de Andrade, A.F., Brasil, S., de-Lima-Oliveira, M., Belon, A.R., Bor-Seng-Shu, E., et al., 2021. Evaluation of cerebral hemodynamics by transcranial Doppler ultrasonography and its correlation with intracranial pressure in an animal model of intracranial hypertension. Arq. De. Neuro Psiquiatr. 80 (4), 344–352.
Sousa Jr., L.M., de Andrade, A.F., Belon, A.R., Soares, M.S., Amorim, R.L., Otochi, J.P., et al., 2016. Evaluation of the maintained effect of 3% hypertonic saline solution in an animal model of intracranial hypertension. Med. Sci. Monit. Basic Res. 22, 123–127.
Steiner, L.A., Czosnyka, M., Piechnik, S.K., Smielewski, P., Chatfield, D., Menon, D.K., et al., 2002. Continuous monitoring of cerebrovascular pressure reactivity allows determination of optimal cerebral perfusion pressure in patients with traumatic brain injury. Crit. Care Med. 30 (4), 733–738.
Taylor, C.A., Bell, J.M., Breiding, M.J., Xu, L., 2017. Traumatic brain injury-related emergency department visits, hospitalizations, and deaths - United States, 2007 and 2013. MMWR Surveill. Summ. 66 (9), 1–16.
Tiba, M.H., McCracken, B.M., Leander, D.C., Colmenero Mahmood, C.I., Greer, N.L., Picton, P., et al., 2022. Trans-Ocular brain impedance indices predict pressure reactivity index changes in a porcine model of hypotension and cerebral autoregulation perturbation. Neurocrit Care 36 (1), 139–147.
Twedt, M., Pfeifer, C., Thorell, W., Bashford, G., 2017. Measuring hemodynamic changes in the ophthalmic artery during applied force for noninvasive intracranial pressure monitoring: test results in a porcine model. Mil. Med. 182 (S1), 72–77.
Virani, S.S., Alonso, A., Benjamin, E.J., Bittencourt, M.S., Callaway, C.W., Carson, A.P., et al., 2020. Heart disease and stroke statistics-2020 update: a report from the american heart association. Circulation 141 (9), e139–e596.